High Energy Processes in Accreting Black Holes
ASP Conference Series, Vol. 161, 1999
Juri Poutanen and Roland Svensson, eds.

ASCA and Radio/RXTE Observations of GX 339-4

M. A. Nowak, J. Wilms[1], J. B. Dove[2], R. P. Fender[3]

JILA, Campus Box 440, Boulder, CO 80309-0440, USA

Abstract. We have analyzed three separate archival Advanced Satellite for Cosmology and Astrophysics (ASCA) observations and eight separate Rossi X-ray Timing Explorer (RXTE) observations of the black hole candidate GX 339−4 in its low luminosity, spectrally hard state. Three of the RXTE observations were strictly simultaneous with 843 MHz and 8.3–9.1 GHz radio observations. All data sets show evidence for an ≈ 6.4 keV Fe line with equivalent widths $\approx$ 20–100 eV. 'Reflection models' show a hardening of the RXTE spectra with decreasing X-ray flux; however, these models do not exhibit evidence of a correlation between the photon index of the incident power law flux and the solid angle subtended by the reflector. None of the models fit to the X-ray data, however, simultaneously explain the observed radio properties. We argue that the spatial extent of the observed radio emission is at least $\mathcal{O}(10^7\ GM/c^2)$. Timing analysis reveals that all observations save one show evidence of a persistent $f_{\rm QPO} \approx 0.3$ Hz QPO. The broad band (10^{-3}–10^2 Hz) power appears to be dominated by two independent processes that can be modeled as very broad Lorentzians with $Q \lesssim 1$. Similar to Cyg X–1, the hard photon variability is seen to lag the soft photon variability with the lag time increasing with decreasing Fourier frequency. The magnitude of this time lag is seen to be positively correlated with the flux of GX 339–4.

1. Introduction

GX 339–4 is a persistent, but highly variable, galactic black hole candidate that shows a wide variety of spectral states. It has an undetermined mass, and lies at a probable distance of ≈ 4 kpc (Zdziarski et al. 1998, and references therein). Here we discuss spectrally hard, low luminosity (3–9 keV flux $\lesssim 10^{-9}$ ergs s^{-1} cm^{-2}) states. We have analyzed three archival ASCA observations and a series of eight RXTE observations, three of which were simultaneous with radio observations (also discussed in Corbel et al. 1998 and Hannikainen et al. 1998). Detailed

[1]Institut für Astronomie und Astrophysik, Abt. Astronomie, Waldhäuser Str. 64, D-72076 Tübingen, Germany

[2]CASA, University of Colorado, Campus 389, Boulder, CO 80309-0389, USA

[3]Astronomical Institute 'Anton Pannekoek', University of Amsterdam, and Center for High Energy Astrophysics, Kruislaan 403, 1098 SJ, Amsterdam, The Netherlands

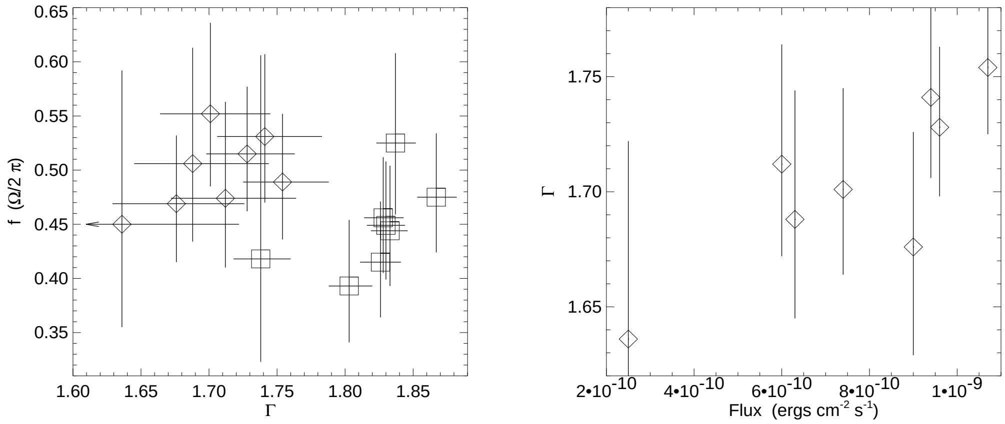

Figure 1. Reflection fraction vs. photon index, Γ, for models fit to PCA data only (squares), and models fit to PCA and HEXTE data simultaneously, but allowing the photon indices and normalizations to be different (diamonds; HEXTE photon index shown). *Right:* Photon index, Γ, vs. observed 3–9 keV flux for the same reflection models as on the left.

discussions of this work can be found in Wilms et al. (1998) and Nowak et al. (1999b).

2. X-ray Observations

We chose to fit the ASCA data with a phenomenological model consisting of a multicolor blackbody spectrum plus a broken power law, considered with and without a narrow Gaussian line at ≈ 6.4 keV. In *all* cases, the inclusion of an Fe line significantly improved the fit (Wilms et al. 1998). The equivalent width of the lines were ≈ 40 eV, even for the faintest observation which had 3–9 keV flux of $\approx 10^{-10}$ ergs s^{-1} cm^{-2}. The detection of an Fe line at such a low flux (along with a soft X-ray excess well-modeled by a power law plus multicolor blackbody with $kT \approx 150$ eV; cf. Wilms et al. 1998) argues against models with extremely large coronal radii of $\mathcal{O}(10^4\ GM/c^2)$ (e.g., Esin, McClintock, & Narayan 1997).

We fit ionized 'reflection models' after Magdziarz & Zdziarski (1995) to our RXTE data. It has been claimed that the best-fit reflection fraction is correlated with the photon index of the incident power law, with softer spectra implying greater reflection (Ueda, Ebisawa, & Done 1994; Zdziarski 1998, this volume). As shown in Fig. 1, we do not see evidence of such a correlation. A linear fit to the correlation is not a statistically significant improvement ($\Delta\chi^2 < 0.8$) over fitting with the mean reflection fraction for *any* of our models. Note that in order to account for systematic differences between the PCA (3–30 keV) and the HEXTE (17–110 keV) instruments on board RXTE, we fit models to the instruments separately. In joint fits of reflection models, we allowed the normalization and slope of the incident power law to be different between the PCA and the HEXTE data (cf. Wilms et al. 1998). [The average difference between the PCA and the

HEXTE data fits was $\Delta\Gamma = 0.12$, with the PCA best fit Crab photon index being 3σ softer and the HEXTE best fit Crab photon index being 1.4σ harder than the $\Gamma = 2.10 \pm 0.03$ photon index found by Toor & Seward (1974); Wilms et al. 1998.] All of our model fits did show, however, that the fainter observations were spectrally harder than the brighter observations (cf. Fig. 1.)

3. Simultaneous Radio Observations

The first three of our RXTE observations were simultaneous with 843 MHz observations taken with the Molongolo Observatory Synthesis Telescope (MOST; cf. Hannikainen et al. 1998), and with 8.3–9.1 GHz observations taken at the Australian Telescope Compact Array (ATCA; cf. Corbel et al. 1998). GX 339−4 showed a nearly flat ($\propto \nu^{0.1-0.2}$) radio spectrum with, typical flux densities of 7 mJy at 843 MHz.

An estimate of the minimum size of the radio emitting region can be obtained by noting that observationally the brightness temperatures of radio sources usually are not larger than 10^{12} K, else the electrons will suffer catastrophic inverse Compton losses. The brightness temperature of a uniformly bright spherical source is given by $(cD/d\nu)^2 S_\nu / 2\pi k$, where d is the diameter of the source, D is its distance, ν is the observed radio frequency, S_ν is the observed radio flux density, c is the speed of light, and k is the Boltzmann constant. GX 339−4 is unresolved in the radio, hence a maximum brightness temperature places a lower limit on the size of the emitting region. Taking the 7 mJy observed at 843 Mz by MOST, we derive

$$d \gtrsim 4 \times 10^{12}\,\mathrm{cm} \left(\frac{D}{4\,\mathrm{kpc}}\right) \approx 5 \times 10^{6}\,R_{\mathrm{G}} \left(\frac{D}{4\,\mathrm{kpc}}\right) \left(\frac{M}{6\,M_\odot}\right)^{-1} . \tag{1}$$

This is far larger than the radius of the corona usually assumed in Comptonization models. The derived size for this system is comparable to that inferred for the radio emission region of other accreting black hole and neutron star systems (cf. Fender & Hendry 1998).

4. Power Spectral Densities

All of the timing analysis was performed in an analogous manner to the timing analysis that we performed for our RXTE observations of Cygnus X–1 (Nowak et al. 1999a). In Fig. 2 we present the power spectral densities (PSD) in the 0–21.9 keV band for our faintest and second brightest observation. All but the faintest observation showed evidence of an ≈ 0.3 Hz QPO. The characteristic 'break frequencies' of the PSD for the faintest observation were approximately a factor of three less than those for the PSD of the brightest observation. The faintest observation also showed greater variability amplitude. We found that all the PSD could be reasonably well-fit by the sum of a power law plus a low-frequency and a high-frequency *broad* Lorentzian (cf. Nowak et al. 1999b). Below, we discuss the implication of such a fit for phenomenological models of the coherence function.

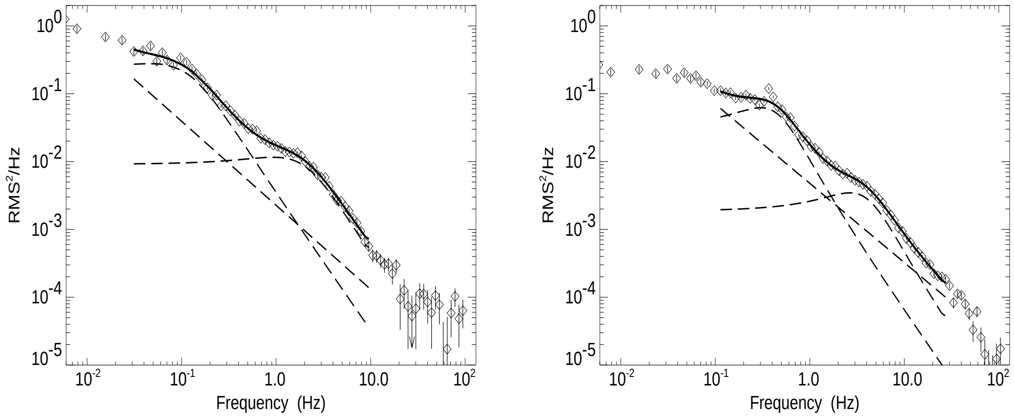

Figure 2. Power spectral densities for our faintest (left) and second brightest (right) RXTE observation of GX 339–4. Solid line is the best fit power law plus two broad Lorentzians. (Fit range is 0.03–10 Hz for the left, and 0.1–30 Hz for the right.) Dashed lines show the individual components of the fits.

5. Coherence Function and Time Lags

We used cross-correlation techniques to compare the variability in the soft and hard X-ray bands. We considered lightcurves in four energy bands: 0–3.9 keV, 3.9–7.5 keV, 7.5–10.8 keV, and 10.8–21.9 keV. The techniques we used are extensively discussed by Vaughan & Nowak (1997) and Nowak et al. (1998a), and references therein. Coherence functions and time lags for the second brightest observation are shown in Fig. 3. Note the 'notch' in the coherence function at ≈ 2 Hz. This notch may indicate that the decomposition of the PSD into a power law plus two Lorentzians may have a physical basis (cf. Nowak et al. 1999b). If each of these individual components represents a process that is coherent with itself (with constant phase lag between hard and soft variability), but that is incoherent with the other two process, then this 'notch', as well as other features of the coherence can be reproduced, as in Fig. 4 (Nowak et al. 1999b).

The one clear trend that we have found for the time lags is that the time-lag between hard and soft X-ray variability grows *shorter* with *decreasing* X-ray flux. We show this trend in Fig. 5. This trend apears to be counter to models where the 'coronal radius' increases with decreasing flux (e.g., Esin, McClintock, & Narayan 1997). Furthermore, considering that the characteristic timescales of the PSD are increased (implying lower PSD frequencies) for lower flux, this trend is counter to energy dependent 'shot noise models' (e.g., Poutanen & Fabian 1999, this volume). The longer shot timescales required to produce lower frequency PSDs should also lead to longer time delays between the hard and soft variability. This trend can be countered to some extent, however, by also varying the characteristic shot spectra as a function of flux, although it is not clear whether the faint and bright spectra are sufficiently different to permit the required change to the individual shot spectra.

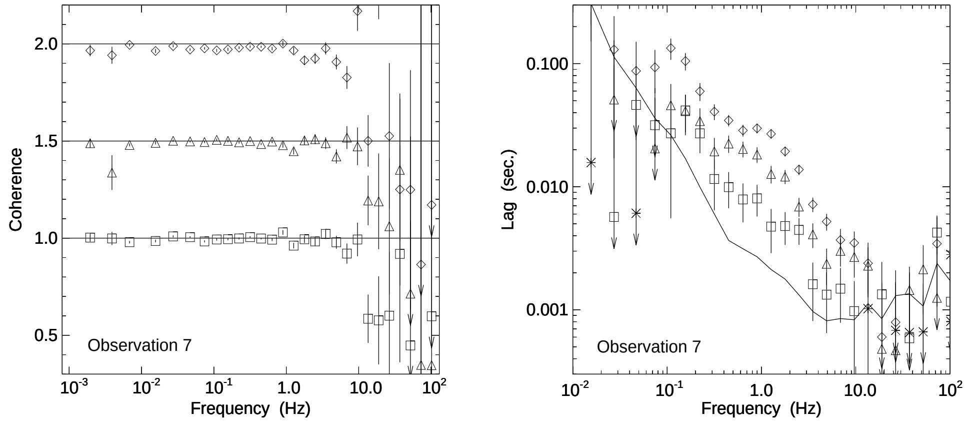

Figure 3. Coherence function (left) and time lags (right) of various energy channels [squares: 3.9–7.5 keV, triangles: 7.5–10.8 keV (coherence offset by 0.5), diamonds: 10.8–21.9 keV (coherence offset by 1.0)] as compared to 0–3.9 keV. Data shown for our second brightest observation. *Left:* Solid lines correspond to unity coherence. *Right:* Crosses are where the soft variability lags the hard variability. Solid line is the Poisson noise level for the 10.8–21.9 keV time lags.

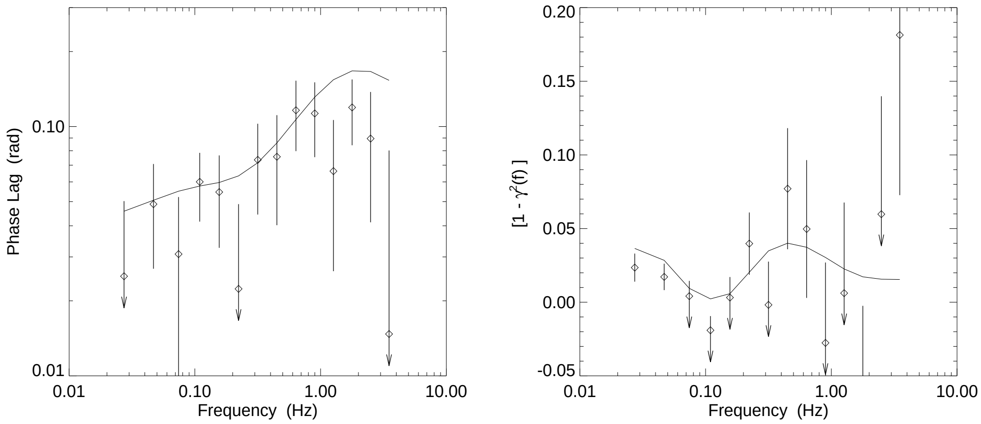

Figure 4. *Left:* Phase lags between 0–3.9 keV and 10.8–21.9 keV variability as a function of Fourier frequency for the faintest observation. (All points are hard variability lagging soft variability.) *Right:* $[1-\gamma_m^2(f)]$, where $\gamma_m^2(f)$ is the measured, noise subtracted coherence function for the same data as on the left. All data has been logarithmically binned over frequencies $f \rightarrow 1.4\ f$. Solid lines are the best fit results obtained by assuming that the power law plus two Lorentzians fit to the PSD are individually coherent, but are incoherent with one another [cf. Nowak et al. 1999b, equations (3) and (4)].

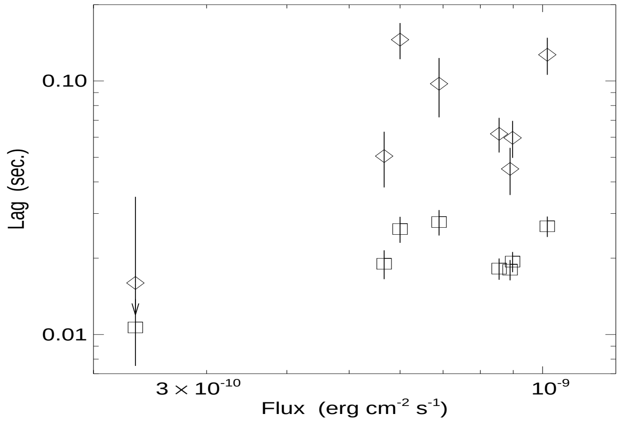

Figure 5. Time lags at Fourier frequencies 0.1 Hz (diamonds) and 0.9 Hz (squares) as a function of measured 3–9 keV flux. Lags are for 10.8–21.9 keV compared to 0–3.9 keV variability.

Acknowledgments. We would like to acknowledge useful conversations with T. Aldcroft, M. Begelman, T. DiMatteo, P. Maloney, K. Pottschmidt, R. Staubert, and B. Vaughan. This work has been financed by NASA Grants NAG5-3225, NAG5-4731, and by a travel grant to J.W. from the DAAD.

References

Corbel, S. et al., 1998, in The 4th Compton Symposium, C. D. Dermer, M. S. Strickman, & J. D. Kurfess, AIP Conf. Proc. Vol. 410, Woodbury, 937

Esin, A. A., McClintock, J. E., & Narayan, R. 1997, ApJ, 489, 865

Hannikainen, D. C., Hunstead, R. W., Campbell-Wilson, D., & Sood, R. K. 1998, A&A, 337, 460

Fender, R. P., & Hendry, M. A. 1998, MNRAS, submitted

Magdziarz, P., & Zdziarski, A. A. 1995, MNRAS, 273, 837

Nowak, M. A., Vaughan, B. A., Wilms, J., Dove, J., & Begelman, M. C. 1999a, ApJ, 510, 874

Nowak, M. A., Wilms, J., & Dove, J. B. 1999b, ApJ, submitted

Poutanen, J., & Fabian, A. 1999, this volume

Toor, A., & Seward, F. D. 1974, AJ, 79, 995

Ueda, Y., Ebisawa, K., & Done, C. 1994, PASJ, 46, 107

Vaughan, B. A., & Nowak, M. A. 1997, ApJ, 474, L43

Wilms, J., Nowak, M. A., Dove, J. B., Fender, R. P., & Di Matteo, T. 1998, ApJ, submitted

Zdziarski, A. A. 1998, this volume

Zdziarski, A. A., Poutanen, J., Mikołajewska, J., Gierliński, M., Ebisawa, K., & Johnson, W. N. 1998, MNRAS, 301, 435